Journal of ELECTRONIC MATERIALS, Vol. 49, No. 10, 2020
https://doi.org/10.1007/s11664-020-08325-1

Crack Effect on the Equivalent Thermal Conductivity of Porously Sintered Silver

FEI QIN,[1,2] YUANKUN HU,[1] YANWEI DAI ,[1,2,3] TONG AN,[1,2] PEI CHEN,[1,2] YANPENG GONG,[1,2] and HUIPING YU[1]

1.—Institute of Electronics Packaging Technology and Reliability, College of Mechanical Engineering and Applied Electronics Technology, Beijing University of Technology, Beijing 100124, China. 2.—Beijing Key Laboratory of Advanced Manufacturing Technology, Beijing University of Technology, Beijing 100124, China. 3.—e-mail: ywdai@bjut.edu.cn

Characterizations of equivalent thermal conductivity (ETC) of sintered silver is an important topic due to the thermal–mechanical reliability requirements of electronic packaging. In this paper, the effect of various types of cracks on the ETC of sintered silver are discussed. A numerical method to simulate the heat transfer behaviors of porous sintered silver containing the crack effect is presented. The results show that the ETC of sintered silver depends significantly on the crack length, crack orientation, porosity, and pore shape. Theoretical formulae to estimate the ETC of sintered silver are also presented, in which the effects of arbitrary crack depth, arbitrary crack orientation, arbitrary porosity, and arbitrary pore shape factor on ETC are included. It has been found that the influence of the side edge crack on the reduction of the ETC of sintered silver is the most obvious compared with the center crack and the upper edge crack. This study presents a quantitative method to evaluate the crack effect on the ETC of porous sintered silver.

Key words: Equivalent thermal conductivity, sintered silver, crack effect, porosity, numerical computation

INTRODUCTION

Sintered silver is a very promising alternative material of the die-attach layer which has drawn much attention in recent years due to its excellent performances.[1] Evaluations of thermomechanical behaviors for sintered silver under various conditions are the main topics which have been investigated by some researchers and engineers,[2–4] as it is the basis of the reliability estimation of sintered silver layers. Due to potential applications of sintered silver as the die-attach layer in power electronics in the next generation, fractures of sintered silver are easily found in experimental works related to thermal mechanical analysis induced by power cycling,[5] which could easily lead to the formation of cracks in sintered silver layers. As the die-attach layer is the main heat dissipater, it is crucial to understand the crack effect on the thermal conduction behaviors of sintered silver when cracks appear.

Some studies have been presented to show the cracking behaviors of sintered silver under various considerations. Tan et al.[6] presented an experimental investigation on the 3D morphology of creep crack growth via an X-ray technique, and they considered that some factors, such as size, shape, and distribution, were important for the growth of creep cracks in sintered silver joints. Shioda and coworkers[7] carried out a low-cycle fatigue investigation on sintered silver and found that fatigue cracks are sensitive to the inelastic energy rate as well as to the sintered temperature. Recent investigations performed by Dai and coworkers[8,9] showed that thermomechanical fatigue damage of sintered silver exhibits mud-crack networks under power cycling tests in which cracks are found with characteristics of high aspect ratios and near-vertical

(Received March 23, 2020; accepted July 8, 2020; published online July 24, 2020)

orientations. However, the crack path is rather different from that of Dai et al.[8,9] according to the investigation by Herboth et al.,[10] in which the crack originates from the corner of the die which grows towards the center of the die-attach layer, and the crack location is inclined and horizontal to the sintered silver die-attach layer. Chen et al.,[11] showed that the fracture toughness of sintered silver increases with the increase in specimen size. Those works are important as they have provided the motivation of the demands on quantitative modeling of the degradation mechanisms of thermomechanical behaviors for sintered silver containing cracks.

Aware of the influence of the microstructure on the thermal conduction of sintered silver, Signor et al.[12] proposed a homogenization method based on the actual 3D microstructure of sintered silver to predict the equivalent thermal conductivity (ETC) of the silver. According to Jose et al.,[13] the ETC of sintered pastes of silver was analyzed by two theoretical methods and measured experimentally. Youssef et al.[14] showed that the thermal conductivity of sintered silver is highly dependent on its porous characteristics, and they performed a computation based on the real morphology of sintered silver. Ordonez-Miranda et al.[15] proposed a differential effective medium theory in which a simple analytical description is given by considering the pores to be ellipsoidal voids of various sizes. Recently, our group[16] reported a microstructure model to predict the ETC of sintered silver considering the aging effect, which reflects the post-sintering effect on the ETC of sintered silver.

Through those studies, one can find that thermomechanical loading easily leads to the formation of cracks in sintered silver. However, different studies have demonstrated that the crack growth path and the crack morphology are different. Note that the sintered silver is the crucial path for heat conduction which can affect the thermal dissipation ability of the die-attach layer. Although it is suspected that the formation of cracks can lead to reliability issues of the die-attach layer, no quantitative investigations are available in the literature to the best of the authors' knowledge. Some questions still remain to be solved, which are listed as follows:

(a) How to build an efficient model which can reflect the crack effect and the characteristics of the microstructure effect on the ETC of sintered silver?
(b) Is there a theoretical model to quantitatively characterize the crack effect on the thermal conduction behaviors of sintered silver?

The aim of this paper is to answer the above two questions. Towards this aim, the organization of this paper is presented as follows. The methodology of the proposed model and the modeling is given in "Model Description" section. In "Theoretical Model and Numerical Scheme" section, the theoretical model to predict the thermal conductivity of sintered silver containing cracks is presented. The results and discussion of the crack effect on the thermal conductivity of sintered silver are given in "Results and Discussion" section. The conclusions are drawn in the last section.

MODEL DESCRIPTION

Characteristics of Sintered Silver Microstructure

A typical characteristic of sintered silver is presented in Fig. 1, where similar characteristics for sintered silver can be found in investigations in Refs.16–18. A nano-porous structure can be found in these sintered silver layers. In order to characterize the distribution characteristics of the sintered silver, the distribution of sintered silver pores were investigated by Gadaud et al.[19] via experiments. It was found that the distribution frequencies of sintered silver pores can be basically assumed to obey the Gaussian law. The specific distribution function is dependent on the sintered processes and the aging condition of the sintered silver.[17]

Recently, a microstructure model with random characteristics of sintered silver pores was proposed by our group which can be adopted to compute the ETC of sintered silver.[16] The basic concept of this numerical method is that the pores are simplified to be circles by satisfying the Gaussian distribution law, i.e., the diameter of the pores in the sintered silver layer are distributed with Gaussian random distribution characteristics. A detailed illustration of the modeling of the sintered silver pores is shown in Fig. 2. The Gaussian fitting can be found in Fig. 2a, and has been illustrated in detail in our previous work.[16] The porosity here is defined as the ratio of the pore area and the model area, where the pores are denoted as the colored circles shown in Fig. 2b.

With the presented pore distribution Gaussian law and modeled sintered silver, the pore characteristics of the sintered silver are obtained. The microstructure obeying Gaussian law is modeled on the MATLAB platform, where the coordinates and diameters of the pores can be obtained. With that information, the microstructure distribution characteristics of the sintered silver model ca be imported into the commercial finite element (FE) code, ABAQUS, to perform thermal analysis to determine the ETC of sintered silver by adding the crack effect.

Modeling of Crack Effect

In order to reflect the crack effect in the microstructure model of the sintered silver layer, a microstructure model containing cracks is proposed.

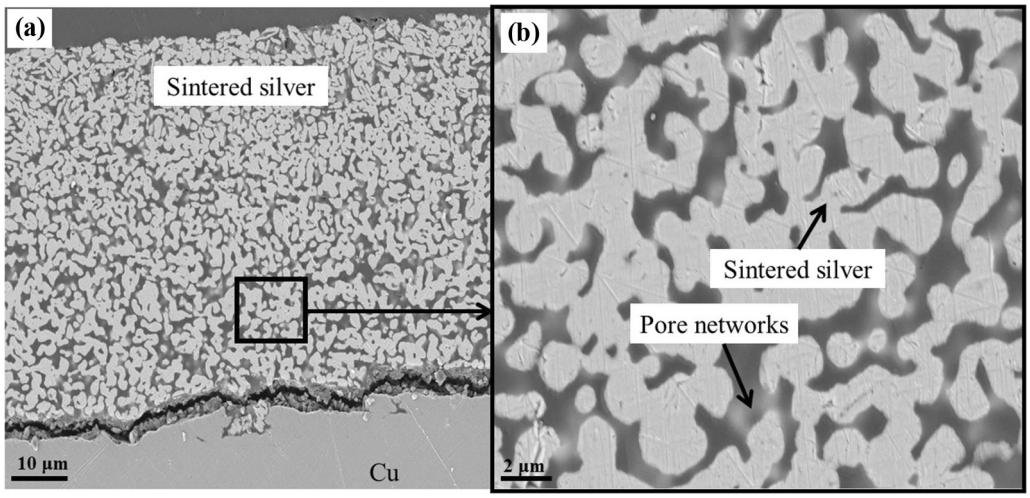

Fig. 1. SEM image of the microstructure for sintered silver layers: (a) microstructure at an overall scale, and (b) microstructure at a local scale.

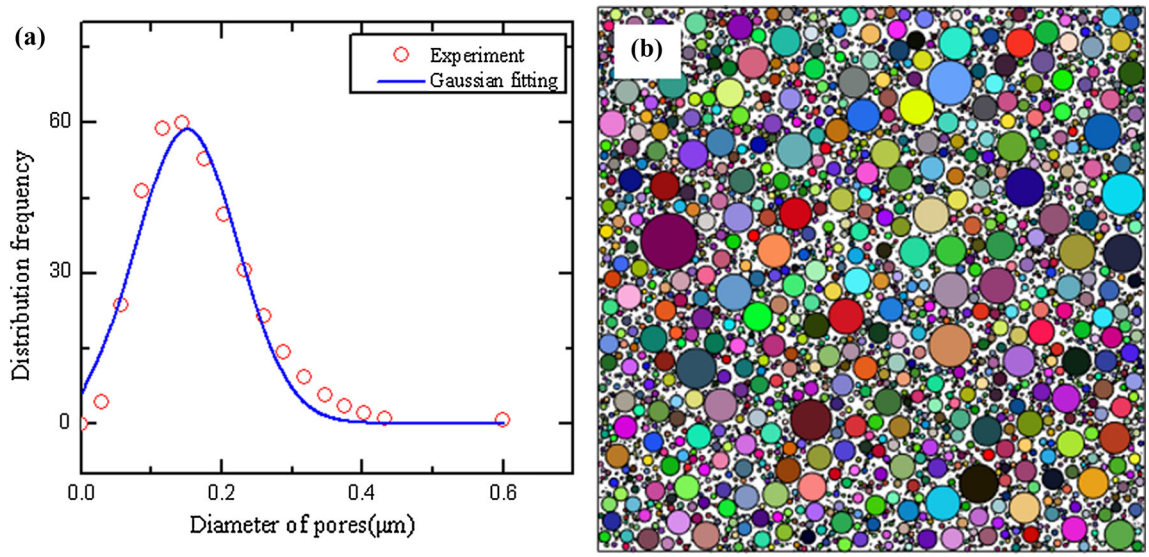

Fig. 2. Modeling of sintered silver: (a) Gaussian fitting of real pore sizes and distributions, and (b) modeled pore distributions.

Each crack is assumed to be a seam. The width of the seam is set at 0.02 μm and the length of the seam varies at the micron level. The crack is considered as a real cut of a seam in the sintered silver layer. In the model, the crack is perfectly straight passing through the sintered silver pores and sintered silver, as shown in Fig. 3. According to the experimental studies,[8] cracks in the sintered silver layer generally appear in three different locations, i.e. at the upper edge, at the side edge, and at the center of the sintered silver layer. The black line shown in Fig. 3 is the crack. In fact, various crack orientation angles have been considered. It should be noted that the crack orientation angle here is defined as the inclined angle between the crack and the horizontal direction. The incline angle is defined as α, as shown in Fig. 3.

THEORETICAL MODEL AND NUMERICAL SCHEME

Although the ETC of sintered silver has been studied based on micromechanics, the crack effect has not been considered. Here, the theoretical model and a numerical scheme considering crack effects are presented as follows.

Prediction of Equivalent Thermal Conductivity for Sintered Silver Containing Cracks

For sintered silver, the ETC prediction form is given here without considering the crack effect, as follows[20]:

$$k_{eq} = k_b(1-\alpha)^n \quad (1)$$

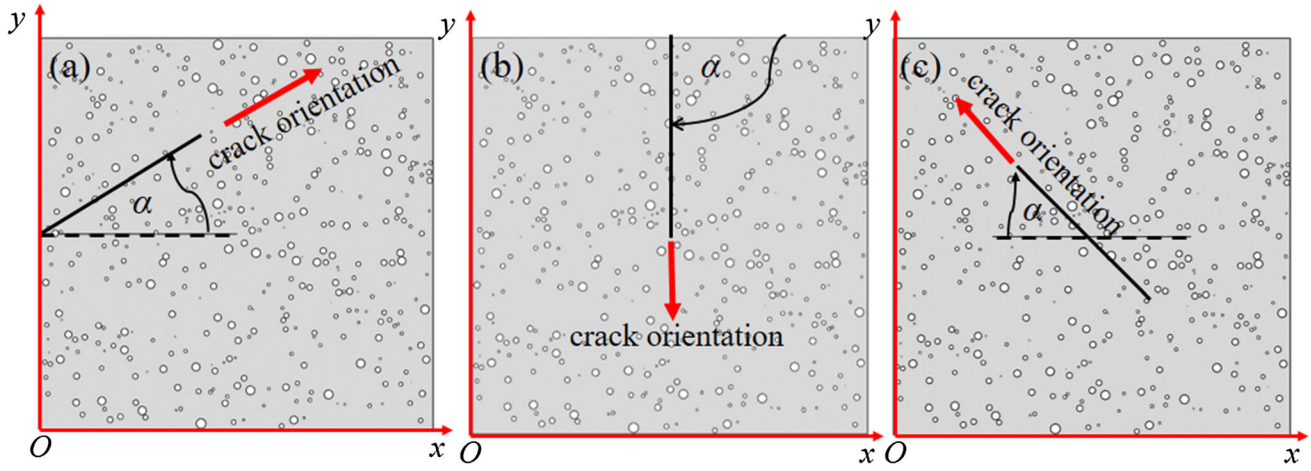

Fig. 3. Three crack models for the sintered silver layer: (a) side edge crack, (b) upper edge crack, and (c) center crack.

where k_b and n are the thermal conductivity of the bulk silver and 1.45 for sintered silver, respectively, according to Gadaud and coworkers.[20] According to the numerical investigation given by Jose and coworkers,[15] the index n adopts different values so as to consider the shape effect of pores on the ETC, e.g., n is 3/2 for spherical pores and 5/3 for cylindrical pores. Except for the above equation, the Maxwell–Eucken model, in which the pore effects on the thermal conductivity is also considered, as follows[21]:

$$k_{\mathrm{eq}}^{\mathrm{Maxwell}} = k_b \frac{2k_b + k_p - 2(k_b - k_p)\varphi}{2k_b + k_p + (k_b - k_p)\varphi}. \tag{2}$$

in which the quantities φ, k_b and k_p are the porosity of the sintered silver, the thermal conductivity of bulk silver, and the thermal conductivity of the pores, respectively.

Recently, we reported a novel form to evaluate the equivalent thermal conductivity of porous sintered silver without considering crack effect, as follows[16]:

$$\frac{1}{k_{eq}} = \frac{\sqrt{\frac{4\varphi}{\pi}}}{k_b + (k_p - k_b)\lambda} + \frac{1 - \sqrt{\frac{4\varphi}{\pi}}}{k_b} \tag{3}$$

in which φ is the porosity of the sintered silver, and λ is a coefficient which is dependent on the distribution uniformity, e.g., the pore shape and the pore distribution uniformity, and it is recommended to adopt between $\sqrt{4\varphi/\pi}$ and $\sqrt{8\varphi/\pi}$. Note that not all the crack effects on the thermal conductivity of sintered silver are considered in these formulae for sintered silver in the available literature.

If the cracks are considered, the influence of crack orientation and crack length should be considered. Hence, the equivalent thermal conductivity of the crack-containing sintered silver is given as:

$$\frac{1}{k_{\mathrm{eq}}^{\mathrm{crack}}} = \left[\frac{\sqrt{\frac{4\varphi}{\pi}}}{k_b + (k_p - k_b)\lambda} + \frac{1 - \sqrt{\frac{4\varphi}{\pi}}}{k_b}\right] \frac{1}{f\left(\frac{a}{W}, \alpha\right)} \tag{4}$$

in which $k_{\mathrm{eq}}^{\mathrm{crack}}$ and $f(a/W,)$ are the equivalent thermal conductivity and correlation coefficient, respectively, k_{eq} is the equivalent thermal conductivity of the sintered silver without cracks, and the correlation coefficient $f(a/W,)$ should be dependent on the crack length, a/W, and its orientation. Hence, the final specific expression of Eq. 4 should be dependent on the crack length and the crack orientation.

Numerical Scheme and Simulation Procedures

Numerical Scheme

In order to obtain the ETC of sintered silver, a numerical scheme is presented as follows. For a homogeneous material, the heat flux with Fourier's law is given as[22,23]:

$$q = -k\frac{\mathrm{d}T}{\mathrm{d}y} \tag{5}$$

in which k, q and T are the thermal conductivity (W/(m K)), heat flux (W/m^2), and temperature (K), respectively. For a homogeneous material, the thermal conductivity is obtained as:

$$k = -\frac{q \cdot \Delta L}{\Delta T} = -\frac{q(y_u - y_l)}{T_u - T_l} \tag{6}$$

where T_u, T_l, y_u and y_l are the temperature of upper boundary, the temperature of lower boundary, and the y-coordinates of the upper and lower boundaries for the calculated sample, respectively.

In order to obtain the ETC, a numerical procedure which has been recently developed by our group is presented here. If Eq. 6 is written in a discrete form

in a two-dimensional condition, Eq. 6 is rearranged as:

$$k = -\frac{q \cdot \Delta L \cdot A}{\Delta T \cdot A} = -\frac{q(y_u - y_l)(\sum_{i=1}^{n} A_i)}{(T_u - T_l) \cdot A} = -\frac{(y_u - y_l)(\sum_{i=1}^{n} q_i A_i)}{(T_u - T_l) \cdot A} \quad (7)$$

in which A is the total area of the computed model and A_i is the area of the i-th cell, and q_i is the heat flux of the i-th cell. The cell can be different shapes, e.g., triangular or quadrilateral. Note that the area, A, of the computed model is identical to $(h_l - h_r)(y_u - y_l)$. Hence, Eq. 7 is rewritten as:

$$k_{\text{eq}} = -\frac{\sum_{i=1}^{n} q_i A_i}{(T_u - T_l) \cdot (x_l - x_r)} \quad (8)$$

where x_l and x_r are the left and right coordinates of the computed model respectively, shown in Fig. 4a.

Note that the ETC of sintered silver given in Eq. 8 is the ETC which does not take the crack effect into account. If the crack effect is considered, the ETC is calculated as:

$$k_{\text{eq}}^{\text{crack}} = -\frac{\sum_{i=1}^{n} q_i A_i + q_{\text{crack}} A_{\text{crack}}}{(T_u - T_l) \cdot (x_l - x_r)} \quad (9)$$

where q_{crack} and A_{crack} are the heat flux and the area of the crack region, respectively.

For the selected cell, it can be independent of its FE meshes (see Fig. 4b), and it can also be dependent on the FE meshes. Here, the cell is attached to the FE meshes. Thus, the area of the cell can be obtained directly through a computation of the element area. A typical FE mesh is shown in Fig. 4. For a triangular element, the heat flux of the element can be obtained through the extraction of the heat flux at the integration point of the element. With the extracted heat flux and the element area, the ETC of sintered silver can be computed through Eq. 9. The element type is a three-node linear transfer triangular element, i.e., DC2D3. The element number here is refined to between 270,000 and 300,000 to obtain a reasonable and convergent solution.

Material Properties and Numerical Procedures

The FE model and FE meshes are shown in Fig. 4, together with the boundary conditions of the simulated model. The temperature attached at the upper and lower boundaries are 250°C and 40°C, respectively. Note that the selection of the temperature at the boundaries does not affect the final computation solutions of the ETC. Hence, the temperature can be

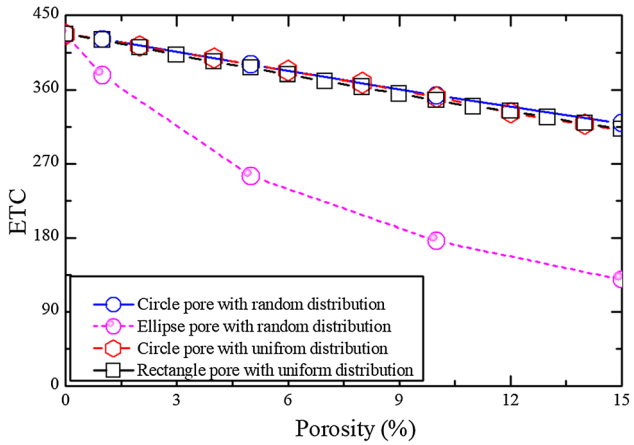

Fig. 5. ETC evaluations with different pore shapes and distributions.

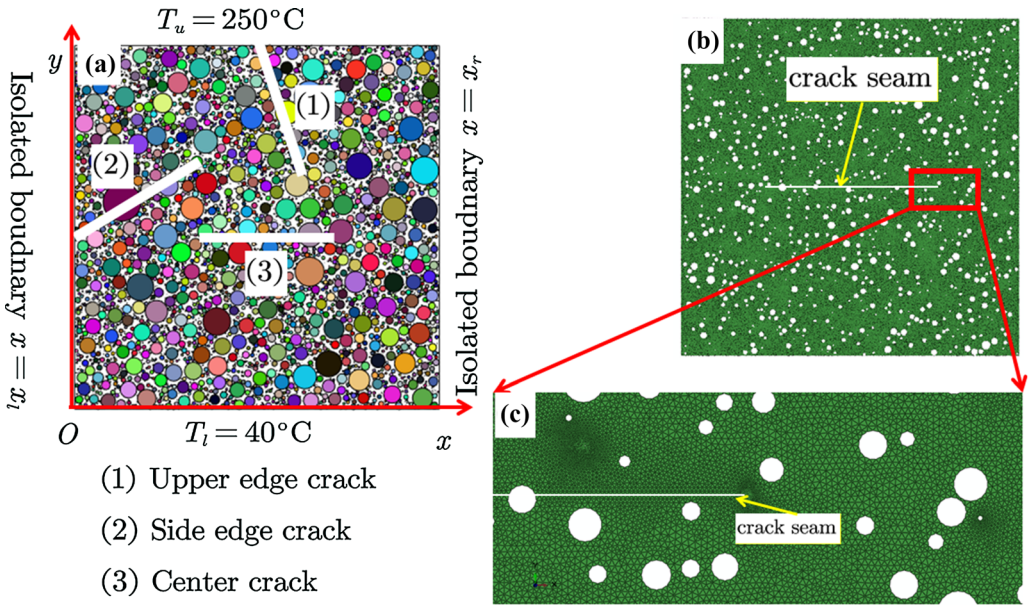

Fig. 4. Configurations of sintered silver: (a) whole computation geometry, (b) entire FE mesh, and (c) local FE mesh.

Table I. Material properties of bulk silver adopted in the simulation

Porosity (%)	Thermal conductivity (W/(m K))	Density (10^3 kg/m^3)	Coefficient of thermal expansion (ppm/°C)
0	429	10.50	~19.2

set to be any number, with the only requirement being that a temperature discrepancy should exist along the upper and lower boundaries. The left and right computation boundaries are assigned with insulated boundaries. For the pore region, the boundaries of the pores are treated as insulated, and the thermal conductivity of air is around 0.0353 W/(m K) at 200°C, according to Wereszczak et al.,[24] which is much less than the thermal conductivity of bulk silver (see Table I).[25] Here, the thermal properties of the bulk silver (i.e., the porosity is equal to 0%) are obtained from Heuck et al.,[25] in which these parameters are adopted in the numerical computations in this work. The thermal conductivity of the crack region is also assigned to 0.0353 W/(m K), i.e., the same as the pore region. With the given material constants, the numerical computations are performed as stated in "Model Description" section. Firstly, the pores are assumed to be distributed randomly with Gaussian distribution satisfied. Secondly, the locations of the pores in the sintered silver are saved via MATLAB. Then, the models of sintered silver with various pores are built through the ABAQUS with the MATLAB information implemented, and the crack is cut at this stage, while thermal analysis is performed at the next stage. The ETC is extracted from ABAQUS via post-processing.

RESULTS AND DISCUSSION

Pore Shape Effect

The microstructures of sintered silver pores are very complex, with spatial networks. The shape of the pores adopted in the simulation may lead to the variations of the evaluation solutions of the ETC. In order to study the pore shape effect on the ETC of sintered silver, three kinds of pore shapes are used to perform the computations, i.e., circles, rectangles and ellipses. The simulation process is the same as that depicted in "Model Description" and "Theoretical Model and Numerical Scheme" sections, except for the adopted pore shape. For elliptical pores, the aspect ratio of the pores is kept as 0.05, being defined as the ratio of the short axis and the long axis.

The variations of the ETC with porosity under various pore shapes are given in Fig. 5. It has been found that the variations tendencies for the ETC with rectangular pores and circular pores are nearly the same regardless of uniform or random distributions. Although the variation tendencies of ETC are nearly the same, the heat flux and temperature distribution are greatly distinguished in the local region due to the local interaction effect of the pores with different shapes. According to the computation solutions given in Fig. 5, the effect of elliptical pores on the reduction of the ETC is more noticeable compared with those of the circular pore and rectangular pores. This implies that the pore shape effect could play a role in the variations of the ETC for sintered silver.

There exist discussions on the pore shape effect on the ETC in sintered silver, e.g., Youssef et al.[14] The shape effect of pores in other porous materials is also available. Kaddouri et al.[26] showed the influence of the pore shape effect on the ETC for inclusion problems. If one adopts the solution given by Kaddouri et al.[26] as the modification factor of the ETC considering the pore shape effect, the ETC of the porous sintered silver layer considering the shape effect of pores is as follows:

$$k_{\mathrm{eq}} = k_{\mathrm{eq}}^{\mathrm{Maxwell}} + 0.7 k_b \varphi(\varphi^2 - 2\varphi + 1)\ln(R) \qquad (10)$$

where φ and R are the porosity ratio and aspect ratio of the pores, respectively. $k_{\mathrm{eq}}^{\mathrm{Maxwell}}$ and k_b are the ETC of the Maxwell model defined in Eq. 2 and the ETC of the pore, respectively.

The comparisons of ETC estimations considering the pore shape effect is presented in Fig. 6, where solutions of different theoretical formulae are presented. Comparing solutions with Eqs. 10 and 3, the prediction solutions with Eq. 1 deviate markedly from the numerical computations regardless of different pore shape factors. For Eq. 1, the values of n of 1.45, 1.50, and 1.68 represent the circular pores, spherical pores and cylindrical pores, respectively. For Eq. 10, four kinds of aspect ratio, R, are given, e.g., 1.0, 0.5, 0.1, and 0.05. The solutions obtained with Eqs. 3 and 10 with $R = 0.05$ agree more closely with the numerical solutions However, the theoretical predictions calculated with various forms all deviate considerably from the numerical solutions. The reason is that the interaction effect of the pores with low aspect ratio is not included in the theoretical formulae; however, the interaction effect can be directly reflected in numerical computations. The ETC heightens if the interaction effect of the pores with a low aspect ratio is considered, which leads to a more noticeable reduction of the ETC.

Side Edge Cracks

The variations of ETC for sintered silver with various side edge crack depths and porosity ratios

are given in Fig. 7. In order to find out the internal relationship of the ETC of sintered silver with crack depth and crack orientation direction, the vertical axial values given in Fig. 5 are normalized as $\eta = k_{eq}^{crack}/k_{eq}$. Here, k_{eq}^{crack} is the ETC of cracked sintered silver and k_{eq} is the ETC of sintered silver without cracks. It is found that the ETC of sintered silver is strongly dependent on the crack length and crack orientation. In detail, the ETC of sintered silver decreases significantly with the increase of crack depth for a specific crack orientation. The smaller the orientation angle, the more obviously the ETC of sintered silver decreases. Otherwise, the ETC of sintered silver decreases with the increase of porosity.

For side edge cracks, the results indicate that the most obvious decrease of ETC of sintered silver occurs when the crack is vertical to the direction of heat transfer (i.e., $\alpha = 0°$). If the crack is parallel to the direction of heat transfer (i.e., $\alpha = 90°$), the ETC does not change that significantly. To reflect the obstruction effect of cracks on the thermal conduction, the temperature distributions under some typical conditions containing cracks are given in Figs. 8 and 9. It can be seen clearly that the crack effect on the decrease of the heat dissipation capability is very noticeable. Differences of crack orientations lead to different temperature distributions even though the porosity is the same. The temperature on the upper crack face is much higher than at other locations, which indicates that the obstruction effect of heat transfer caused by the formation of cracks makes the ability of heat conduction worse. It also indicates that the

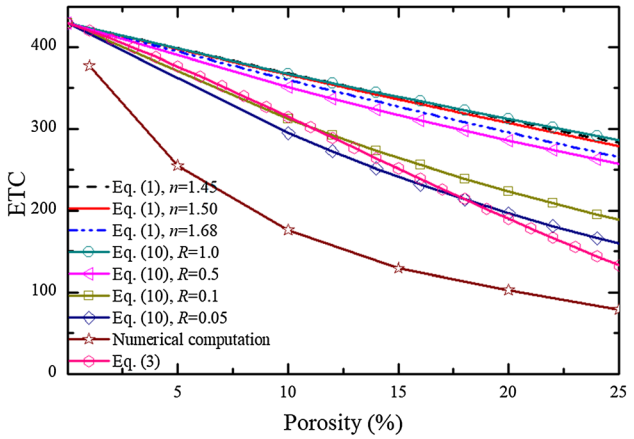

Fig. 6. ETC estimations considering the pore shape effect.

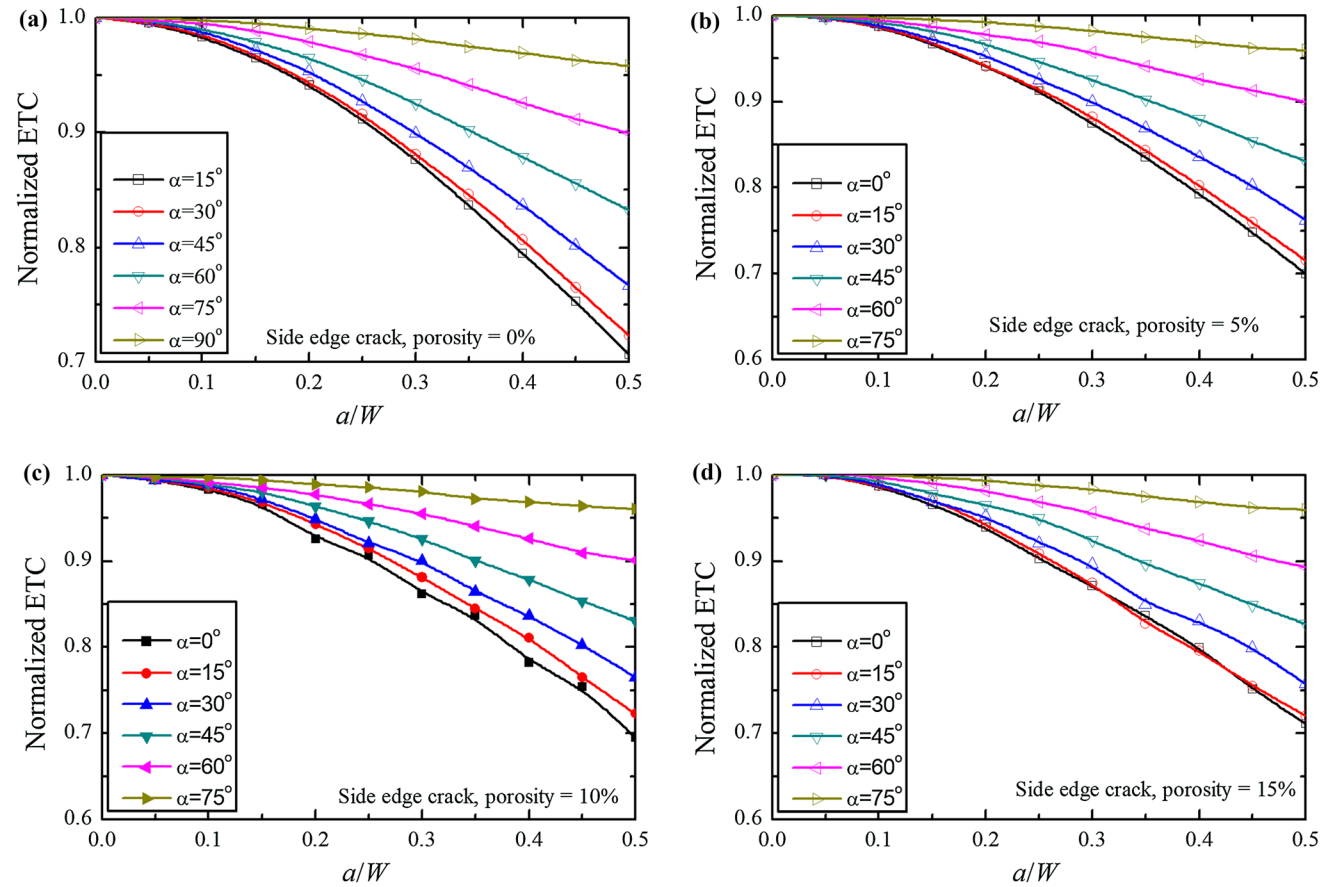

Fig. 7. Variations of equivalent thermal conductivity with different crack depths and crack orientations for side edge cracks under various porosities: (a) 0%, (b) 5%, (c) 10%. and (d) 15%.

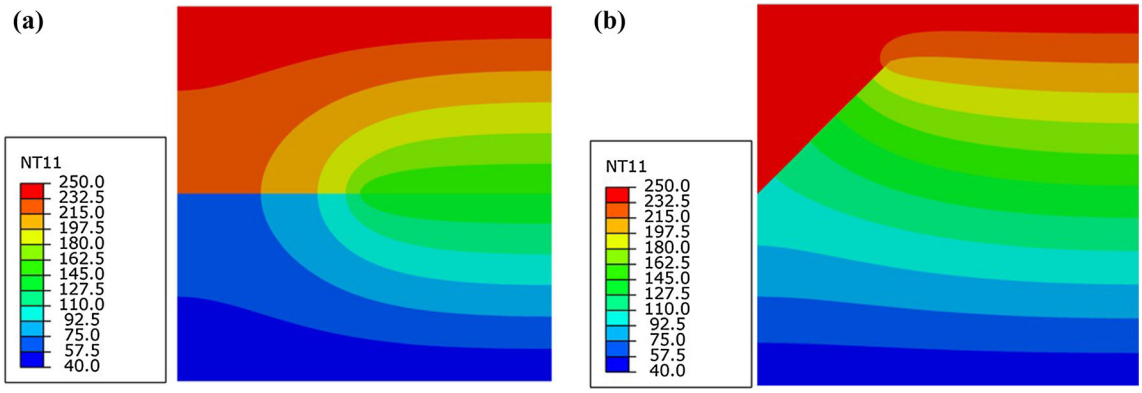

Fig. 8. Distributions of temperature for sintered silver under a porosity of 0% with crack orientation angles: (a) 0° and (b) 45°.

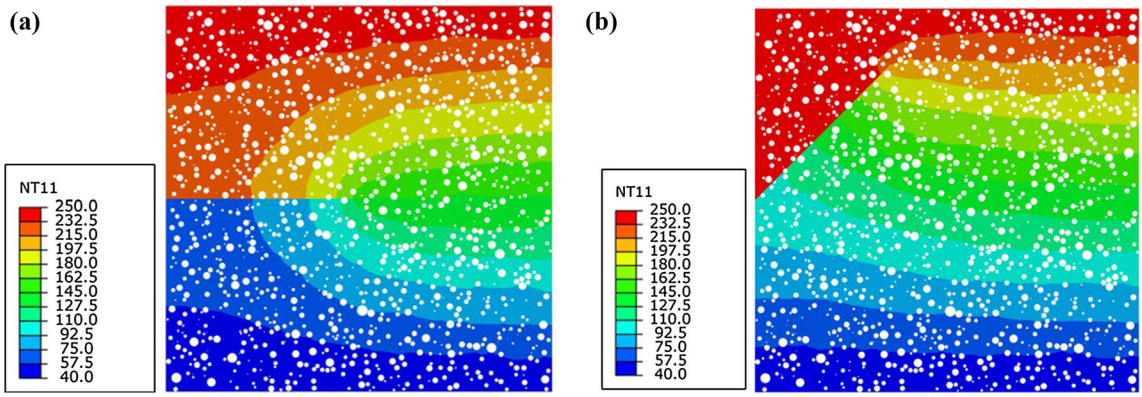

Fig. 9. Distributions of temperature for sintered silver under a porosity of 15% with side edge crack orientation angles: (a) 0° and (b) 45°.

formation of cracks leads to the change of the temperature gradient along the heat transfer direction.

Center Cracks

Except for side edge cracks, center cracks can also appear during the service of the sintered silver layer. The variations of the ETC of sintered silver with different center crack depths under various crack orientations are presented in Fig. 10. Compared with the side edge crack effect, similar tendencies can be found for center cracks. It is found that the ETC of sintered silver is also strongly dependent on the crack length and crack orientation for center cracks. It is also found that the ETC of sintered silver decreases significantly with the increase of crack depth if the crack orientation is fixed. If the crack length is small, the crack effect on the discrepancy of ETC is smaller. For larger crack lengths, the effect of crack orientation is more obvious. Different porosities also play an important role in the variations of the ETC.

For center cracks, the results show that the most noticeable reduction of the ETC for sintered silver occurs when the crack is vertical to the direction of heat transfer (i.e., $\alpha = 0°$). If the crack is parallel to the direction of heat transfer (i.e., $\alpha = 90°$), the ETC is kept as nearly constant and can only be affected by the porosity. The temperature distributions containing center cracks with orientations $\alpha = 90°$ and $\alpha = 90°$ are given in Figs. 11 and 12, respectively, where two different porosities are considered. Compared with side edge cracks, the temperature distributions of center cracks are also different.

Upper Edge Cracks

The variations of the ETC of sintered silver with different crack depths under various crack orientations for upper edge cracks are presented in Fig. 13. Compared with the side edge crack effect and center cracks, similar tendencies can also be found for upper edge cracks. It is found that the ETC of sintered silver is also strongly dependent on the crack length and crack orientation for upper edge cracks. The ETC of sintered silver decreases significantly with the increase of crack depth if the crack orientation is fixed. If the crack length is small, the crack effect on the discrepancy of the ETC is not obvious. For larger crack lengths, the effect of the direction of crack orientation is more significant. Different porosities also play an important role in the contribution to the variations of the ETC.

The effect of upper edge cracks on temperature distributions of sintered silver is presented in

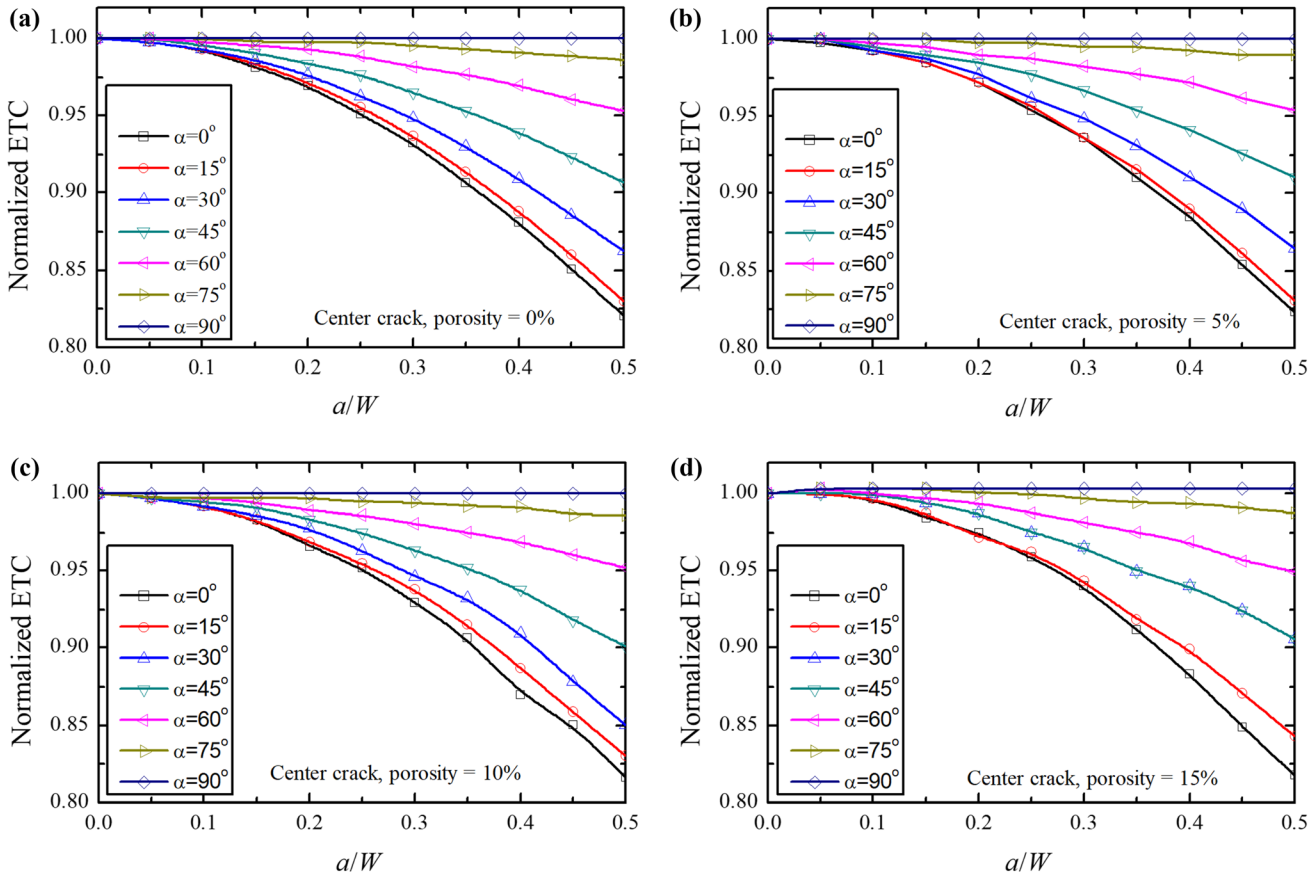

Fig. 10. Variations of ETC with different crack depths and crack orientations for center cracks under various porosities: (a) 0%, (b) 5%, (c) 10%, and (d) 15%.

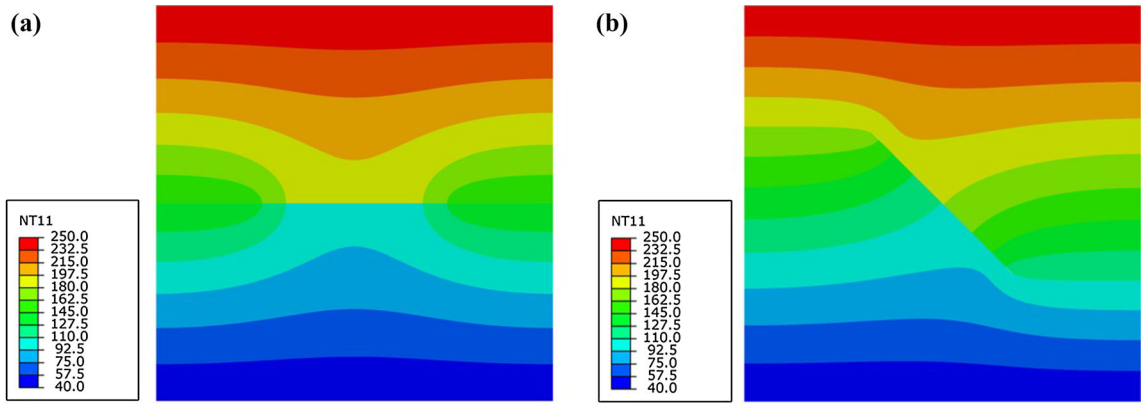

Fig. 11. Distributions of temperature for sintered silver under a porosity of 0% with orientation angles: (a) 0° and (b) 45°.

Figs. 14 and 15. It can be seen that the obstruction of cracks on the ETC of sintered silver varies as the crack orientation changes. For $\alpha = 90°$, the obstruction effect of cracks on ETCs is almost negligible. For $\alpha = 45°$, it I can be clearly seen that the temperature distributions are different compared with that of $\alpha = 90°$.

Discussion

Crack Location Effect

Although the variations of different ETCs with crack depth ratio have been presented in "Pore Shape Effect–Center Crack" sections, the detailed influences of the appearance of crack locations on the ETC of sintered silver are obviously different, as shown in Fig. 16. The most significant influence of

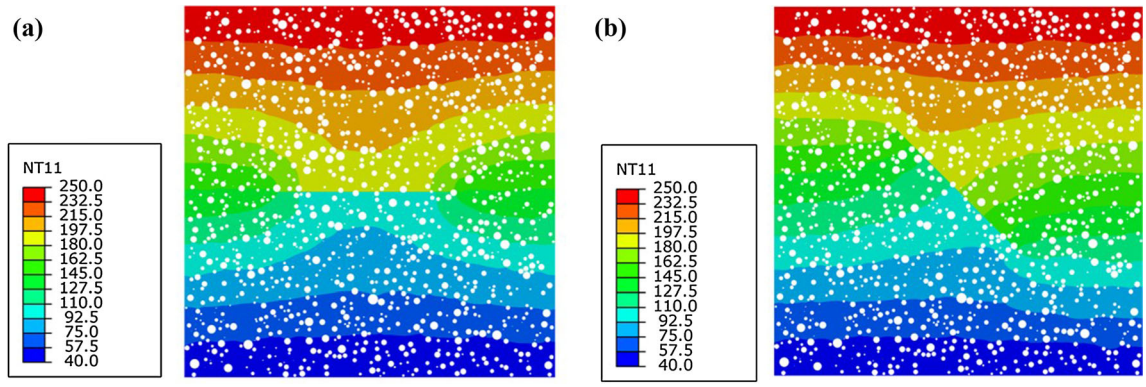

Fig. 12. Distributions of temperature for sintered silver under a porosity of 15% with orientation angles: (a) 0° and (b) 45°.

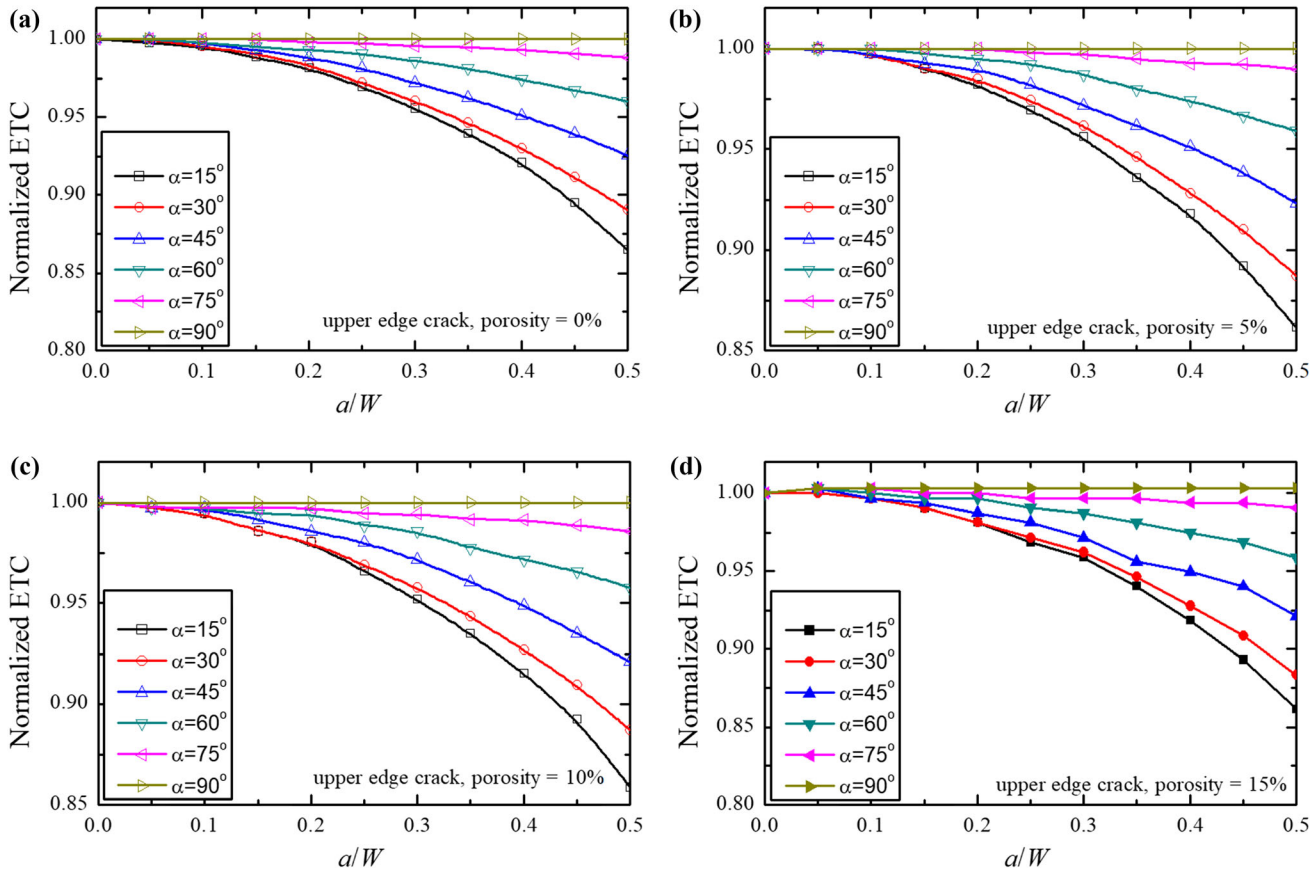

Fig. 13. Variations of ETC with different crack depths and crack orientations for upper edge cracks under various porosities: (a) 0%, (b) 5%, (c) 10%, and (d) 15%.

cracks on the decrease of the ETC for sintered silver with various porosities is by the side edge crack. The weakest effect of cracks on the ETC of sintered silver is by the upper edge crack. The discrepancy of the crack effect on the ETC of sintered silver among the three crack types can approach 19.68%, i.e., the condition in Fig. 16a. This indicates that side edge cracks on the ETC are more significant than the other types of crack, implying that the obstacle effect of side edge cracks on heat dissipation of sintered silver is more important.

From the above investigations, some useful guidelines can be provided. The formation of side edge cracks should be avoided during the service of the sintered silver layer as it can make the heat conduction become even worse compared with other types of cracks. A vertical crack is more preferable than a horizontal crack as the heat conduction

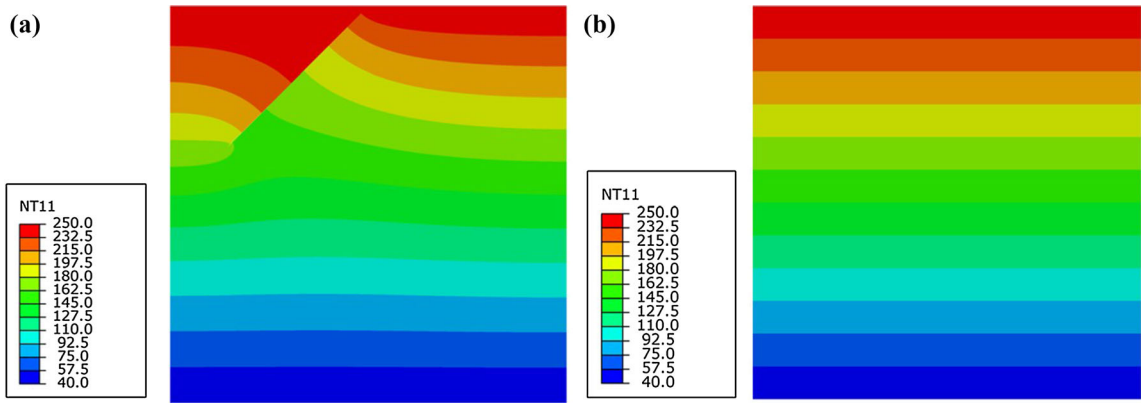

Fig. 14. Distributions of temperature for upper edge cracks within sintered silver under a porosity of 0% with orientation angles: (a) 0° and (b) 45°.

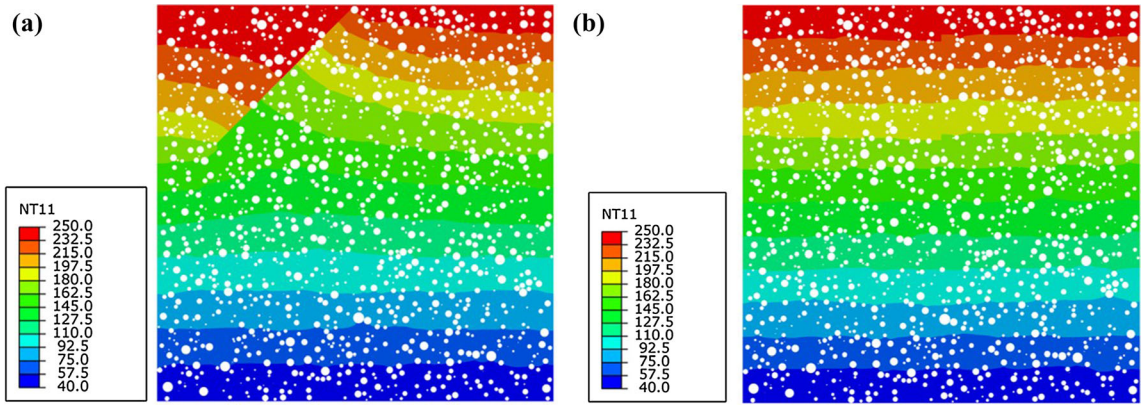

Fig. 15. Distributions of temperature for upper edge crack within sintered silver under a porosity of 15% with orientation angles: (a) 0° and (b) 45°.

ability of the sintered silver layer with a vertical crack is better.

Fitting Estimation Formula of Equivalent Thermal Conductivity with Cracks

The results of a normalized ETC given for different types of cracks discussed in "Pore Shape Effect–Center Crack" sections show that the normalized ETC varies nonlinearly with the increase of dimensionless crack length, a/W. Here, polynomial fittings of the data show that the variations of a normalized ETC with a/W can be predicted with the following formula:

$$\frac{k_{\mathrm{eq}}^{\mathrm{crack}}}{k_{\mathrm{eq}}} = \beta_1\left(\frac{a}{W}\right)^3 + \beta_2\left(\frac{a}{W}\right)^2 + \beta_3\left(\frac{a}{W}\right) + 1 \qquad (11)$$

in which the coefficients β_1, β_2 and β_3 are considered to be dependent on the crack orientation. As a typical condition, the comparisons of the computed ETC and fitting solutions with Eq. 12 for sintered silver with two porosities are given in Fig. 16, from which it can be seen that the fitting solutions agree quite well with the numerical computations of the scheme given in "Numerical Scheme" section. In fact, the fitting solutions have been compared with all the computational results. The solutions fitted with Eq. 11 all agree quite well with the numerical solutions regardless of variations of porosity. The coefficients of β_1, β_2 and β_3 for Figs. 17a and b are listed in Tables II and III, respectively. From Eq. 12 and the solutions given in Tables II and III, the errors between the calculated solutions and the fitting solutions are controlled to be under 3%. This indicates that the proposed Eq. 11 can be used to predict the ETC quite reasonably under various porosities.

Analytical Estimation Formula of ETC Considering Crack Effects for Sintered Silver

Although Eq. 11 can be adopted to predict the variation of the ETC for some special cases, it cannot be easily extended to other conditions. Hence, an analytical formula is still needed. Based on the solutions given previously in "Pore Shape Effect–Upper Edge Crack" section, a prediction formula can be given in the following formula based on Eq. 4:

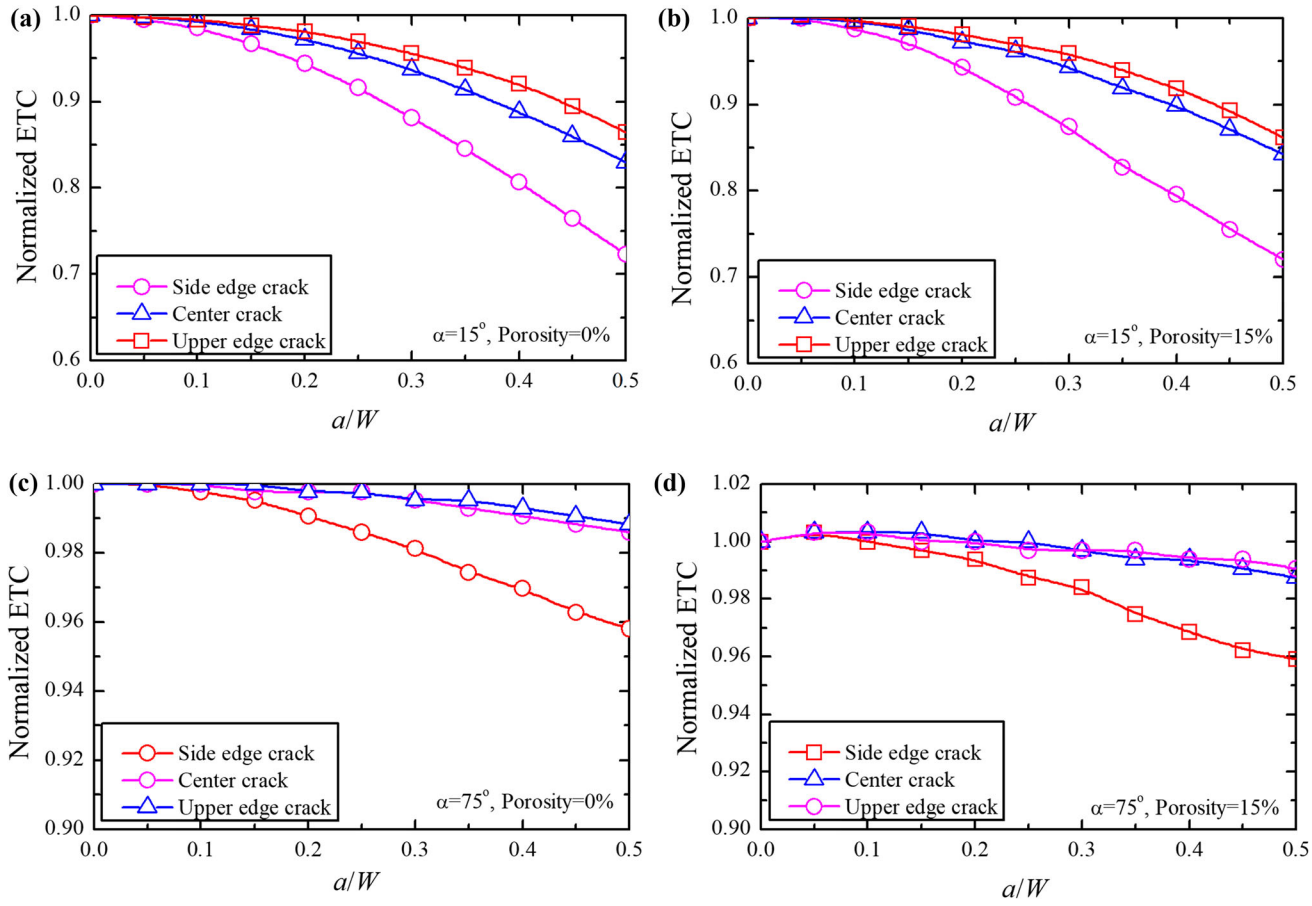

Fig. 16. Comparisons of ETC for different crack types.

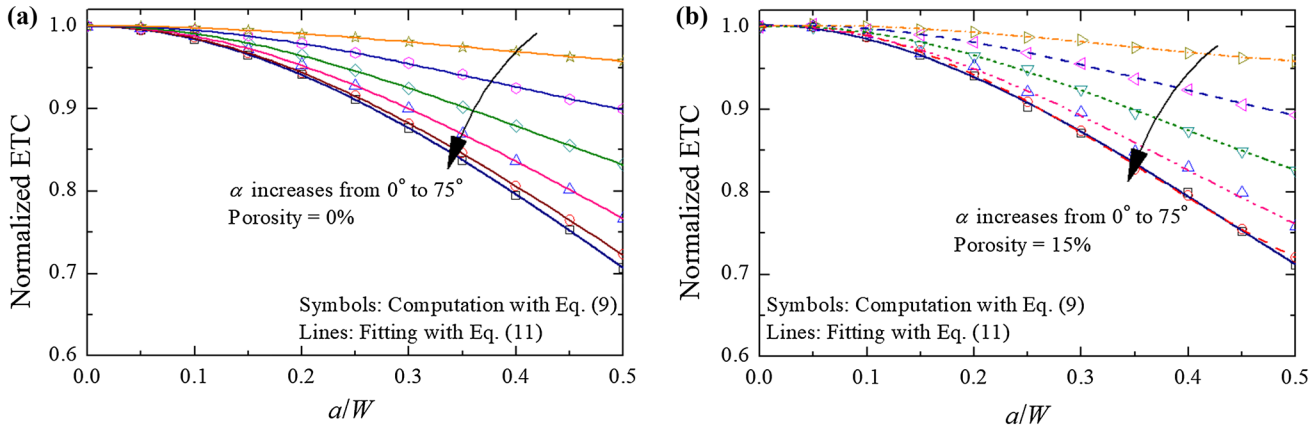

Fig. 17. Comparisons of computed ETCs and fitting curves with Eq. 11 for different porosities: (a) 0% and (b) 15%.

Table II. Fitting coefficients for curves in Fig. 16a

Porosity (%)	Crack orientation α (°)	β_1	β_2	β_3
0	0	0.3007	− 0.3407	0.0107
0	15	0.6955	− 0.8183	0.0346
0	30	0.9328	− 1.1851	0.0227
0	45	0.9708	− 1.441	0.0113
0	60	1.0577	− 1.6616	0.012
0	75	1.0251	− 1.6936	0.0042

Table III. Fitting coefficients for curves in Fig. 16b

Porosity (%)	Crack orientation α (°)	β_1	β_2	β_3
15	0	0.5424	− 0.5446	0.0527
15	15	0.8552	− 0.9947	0.0674
15	30	1.2412	− 1.4528	0.0691
15	45	1.5735	− 1.8428	0.0486
15	60	2.4727	− 2.6433	0.1453
15	75	1.3927	− 1.8626	0.0021

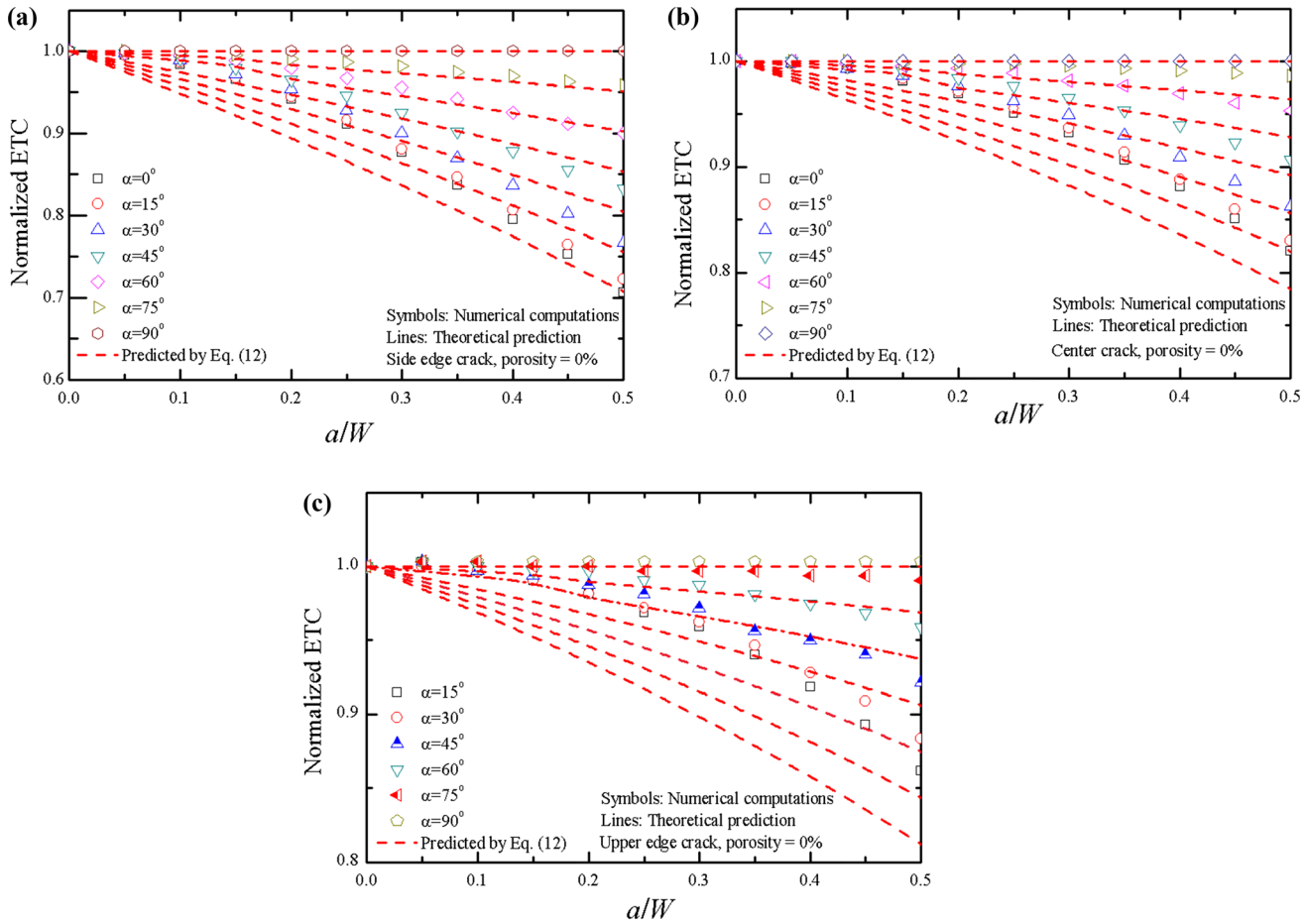

Fig. 18. Comparisons of computed ETCs and theoretical predictions with Eq. 12.

$$k_{\mathrm{eq}}^{\mathrm{crack}} = k_{\mathrm{eq}} \frac{\alpha - \left(\alpha - \frac{\pi}{2}\right)\left(1 - \frac{a}{W}\right)^n}{\frac{\pi}{2}} \tag{12}$$

where α and a/W are the inclined angle of the crack and the crack length, respectively, indicating that the coefficient of Eq. 4 is identical to the following:

$$f\left(\frac{a}{W}, \alpha\right) = \frac{\alpha - \left(\alpha - \frac{\pi}{2}\right)\left(1 - \frac{a}{W}\right)^n}{\frac{\pi}{2}} \tag{13}$$

Here, n adopts the following values according to different crack types, e.g., side edge crack, center crack, and upper edge crack:

$$n = \begin{cases} 0.5 & \text{for side edge crack} \\ 0.35 & \text{for center crack} \\ 0.3 & \text{for upper edge crack} \end{cases} \tag{14}$$

Comparisons of the theoretical prediction of the ETC with Eq. 12 and numerical computations are given in Fig. 18, from which it can be clearly seen

that all the computed solutions have the same tendencies as that given in analytical Eq. 12. As mentioned previously, the exponent n in Eq. 5 still needs to be determined. For deep cracks, the discrepancies of the ETC between the prediction solutions with Eq. 12 and the numerical solutions are quite large. However, the ETC of the predicted solutions with Eq. 12 and the numerical computations are much closer. Generally, Eq. 12 can be used to predict the ETC of sintered silver containing cracks with different porosities under various conditions. The estimated solutions of Eq. 12 can be selected as the lower bound for the evaluation of ETCs in engineering practices.

If one considers both the pore shape effect and the crack effect in the evaluation of ETCs, the ETC is expressed as the following, based on Eq. 12:

$$k_E^{\text{crack}} = \frac{\left[k_{\text{eq}}^{\text{Maxwell}} + 0.7k_b\varphi(\varphi^2 - 2\varphi + 1)\ln(R)\right]\left[\alpha - (\alpha - \frac{\pi}{2})(1 - \frac{a}{W})^n\right]}{\frac{\pi}{2}} \tag{15}$$

where the quantities represent the same physical meanings as those defined in Eq. 10. The values of n depend on the crack types as defined in Eq. 14. With Eq. 15, the effect of pore shape and crack effect on the ETC are all included, indicating that the ETC can be estimated through Eq. 15 with arbitrary porosity, arbitrary crack length, arbitrary crack orientation, and arbitrary pore shape.

CONCLUSIONS

The influences of crack effects on the equivalent thermal conductivity (ETC) of sintered silver with porous characteristics have been investigated. Based on the theoretical analysis and numerical computation, the following conclusions can be drawn:

1. A numerical method to compute the ETC of sintered silver containing realistic cracks has been presented. This method has been verified to reasonably reflect the obstacle effect of cracks on the heat conduction in sintered silver. The most significant effect of crack orientation on the decrease of ETC for sintered silver occurs in a direction which is vertical to the heat conduction. For cracks parallel to the direction of the heat conduction, the crack effect is negligible. It has been found that the variations of the ETC of sintered silver is strongly dependent on the crack location, crack depth, crack orientation, porosity, and pore shape.
2. A theoretical formula has been presented to characterize the crack effect on the ETC of sintered silver. Analytical expressions to characterize the ETC of sintered silver are given, which presents reasonable tendencies with the numerical solutions. The presented formula can be adopted to characterize the ETC of sintered silver with arbitrary crack depth, arbitrary crack location, arbitrary porosity, and arbitrary pore shape. Note that the presented theoretical form cannot take the interaction effect of pores into account; however, the numerical method can encompass the interaction effect of pores with different shapes.
3. Three different kinds of crack position effects on the ETC of sintered silver are presented. It has been found that the side edge crack possesses the most noticeable influence on the reduction of the ETC of sintered silver compared with the center crack and the upper side edge crack. This can provide some guidelines on the design and optimization of the thermal behaviors of the sintered silver layer, e.g., horizontal cracks should be avoided for sintered silver compared with vertical cracks as the obstruction effect of horizontal cracks on heat conduction is much more obvious.

ACKNOWLEDGMENTS

The authors acknowledge the support from the National Natural Science Foundation of China (11902009 and 11672009), the Beijing Natural Science Foundation (2204074), the Scientific Research Common Program of Beijing Municipal Commission of Education (KM202010005034), the China Postdoctoral Science Foundation (2019M650403) and the Chaoyang District Postdoctoral Science Foundation (2019ZZ-47).

CONFLICT OF INTEREST

The authors declare that they have no conflict of interest.

REFERENCES

1. C. Chen, S. Nagao, H. Zhang, J. Jiu, T. Sugahara, K. Suganuma, and K. Tsuruta, *J. Electron. Mater.* 46, 1576 (2017).
2. Y.H. Mei, G. Chen, X. Li, G.Q. Lu, and X. Chen, *Solder Surf. Mt Tech.* 25, 107 (2013).
3. K.S. Siow, *J. Electron. Mater.* 43, 947 (2014).
4. Y. H. Mei, Z. Wang, K.S. Siow, in Die-Attach Materials for High Temperature Applications in Microelectronics Packaging, ed. by Siow and Kim Shyong (Springer, Cham, 2019), p. 125–150.
5. R. Kimura, Y. Kariya, N. Mizumura and K. Sasaki, *Mater Trans*, M2017392 (2018).
6. Y. Tan, X. Li, G. Chen, Y.H. Mei, and X. Chen, *J. Electron. Mater.* 44, 761 (2015).
7. R. Shioda, Y. Kariya, N. Mizumura, and K. Sasaki, *J. Electron. Mater.* 46, 1155 (2017).
8. P. Agyakwa, J. Dai, J. Li, B. Mouawad, L. Yang, M. Corfield, and C.M. Johnson *J Microsc-Oxford*. 0(0), 1 (2019).
9. J. Dai, J. Li, P. Agyakwa, M. Corfield, and C.M. Johnson, *IEEE T Device Mater. Reliab.* 18, 256 (2018).
10. T. Herboth, M. Guenther, A. Fix, and J. Wilde *in 2013 IEEE 63rd Electronic Components and Technology Conference*, 1621 (2013).
11. C. Chen, S. Nagao, K. Suganuma, J. Jiu, T. Sugahara, H. Zhang, and K. Tsuruta, *Acta Mater.* 129, 41 (2017).
12. S. Sakamoto, T. Sugahara, and K. Suganuma, *J. Maters. Sci. Mater. Electron.* 24, 1332 (2013).

13. J. Carr, X. Milhet, P. Gadaud, S.A. Boyer, G.E. Thompson, and P. Lee, *J. Mater. Process Technol.* 225, 19 (2015).
14. T. Youssef, W. Rmili, E. Woirgard, S. Azzopardi, N. Vivet, D. Martineau, and C. Richard, *Microelectron. Reliab.* 55, 1997 (2015).
15. J. Ordonez-Miranda, M. Hermens, I. Nikitin, V.G. Kouznetsova, O. van der Sluis, M.A. Ras, and C.S. Torres, *Int. J. Therm. Sci.* 108, 185 (2016).
16. F. Qin, Y.K. Hu, Y.W. Dai, T. An, and P. Chen, *Microelectron. Reliab.* 108, 113633 (2020).
17. S.A. Paknejad and S.H. Mannan, *Microelectron. Reliab.* 70, 1 (2017).
18. K.S. Siow and S.T. Chua, *Met. Mater. Int.* (2019). https://doi.org/10.1007/s12540-019-00394-0.
19. X. Long, B. Hu, Y. Feng, C. Chang, and M. Li, *Int. J. Mech. Sci.* 161, 105020 (2019).
20. P. Gadaud, V. Caccuri, D. Bertheau, J. Carr, and X. Milhet, *Mater. Sci. Eng. A* 669, 379 (2016).
21. I. Sumirat, Y. Ando, and S. Shimamura, *J. Porous. Mater.* 13, 439 (2006).
22. A. El Moumen, T. Kanit, A. Imad, and H. El Minor, *Comp. Mater. Sci.* 97, 148 (2015).
23. H.S. Carslaw and J.C. Jaeger, 2nd Edition. (Clarendon, Oxford, 1959), pp. 1–84.
24. A.A. Wereszczak, D.J. Vuono, H. Wang, M.K. Ferber, and Z. Liang, Properties of Bulk Sintered Silver as a Function of Porosity (No. ORNL/TM-2012/130), Oak Ridge National Lab. (ORNL), Oak Ridge, TN, USA, (2012).
25. N. Heuck, A. Langer, A. Stranz, G. Palm, R. Sittig, A. Bakin, and A. Waag, *IEEE Trans. Compon. Pack Manuf.* 1, 1846 (2011).
26. W. Kaddouri, A.E. Moumen, T. Kanit, S. Madani, and A. Imad, *Mech. Mater.* 92, 41 (2016).